ORIGINAL PAPER

CRYSTAL Research & Technology

www.crt-journal.org

The Impact of AlN Templates on Strain Relaxation Mechanisms during the MOVPE Growth of UVB-LED Structures

Arne Knauer, Anna Mogilatenko, Jonas Weinrich, Sylvia Hagedorn, Sebastian Walde, Tim Kolbe, Leonardo Cancellara, and Markus Weyers*

Strain relaxation mechanisms in AlGaN based light emitting diodes emitting in the ultraviolet B spectral range (UVB-LEDs) grown on different AlN/sapphire templates are analyzed by combining in situ reflectivity and curvature data with transmission electron microscopy. In particular, the impact of dislocation density, surface morphology, and lattice constant of the AlN/sapphire templates is studied. For nonannealed AlN/templates with threading dislocation densities (TDDs) of 4×10^9 and 3×10^9 cm^{-2} and different surface morphologies strain relaxation takes place mostly by conventional ways, such as inclination of threading dislocation lines and formation of horizontal dislocation bands. In contrast, a TDD reduction down to 1×10^9 cm^{-2} as well as a reduction of the lattice constant of high temperature annealed AlN template leads to drastic changes in the structure of subsequently grown AlGaN layers, e.g., to transformation to helical dislocations and enhanced surface enlargement by formation of macrofacets. For the growth of strongly compressively strained AlGaN layers for UVB-LEDs the relaxation mechanism is strongly influenced by the absolute values of TDD and the lattice constant of the AlN templates and is less influenced by their surface morphology.

1. Introduction

The wide field of applications for light emitting diodes (LEDs) emitting in the ultraviolet (UV) spectral region as, e.g., curing of polymers, phototherapy, medical diagnostics, plant growth lighting, sensing, disinfection of water, and so on,[1,2] calls for development of more efficient InAlGaN based heterostructures. Although a lot of progress has been made in the performance of UV-LEDs, the efficiency and operating voltage of the devices as well as their lifetime still need to be improved. One precondition for the improvement of the efficiency of UV-LEDs is the reduction of dislocation density in the active area of these structures to the low 10^8 cm^{-2} range[3,4] because dislocations act as nonradiative recombination centers. Due to the lack of inexpensive, transparent native AlN substrates nearly all UV-LEDs are grown on AlN/sapphire templates. One challenge in AlN growth on sapphire is that the layers are always heavily strained due to their large lattice and thermal mismatch to the sapphire. This high mismatch as well as the not perfect alignment between the AlN nuclei formed at the start of heteroepitaxial growth generally causes threading dislocation densities (TDDs) much higher than 10^9 cm^{-2}. Since the group of Miyake[5–7] showed the possibility of decreasing the TDD of AlN/sapphire templates down to 2×10^8 cm^{-2} by high temperature annealing (HTA), many groups tried to grow UV-LED structures on such low dislocation density templates and found this to be challenging,[8–10] especially for LED structures emitting in the UVB region (UVB-LEDs). Here the Al-mole fraction of the (In)AlGaN layers of the active region is below 40% making pseudomorphic growth on AlN templates impossible due to the high compressive strain. To avoid the formation of defects in the active region of the LED the underlying AlGaN layer needs to be simultaneously relaxed and of good crystalline quality. Thus, in situ assessment of strain development during the heterostructure growth and of relaxation mechanisms such as cracking, dislocation formation, or surface roughening is very important for process optimization.

Dr. A. Knauer, Dr. A. Mogilatenko, J. Weinrich, Dr. S. Hagedorn, S. Walde, Dr. T. Kolbe, Prof. M. Weyers
Ferdinand-Braun-Institut
Leibniz-Institut fuer Hoechstfrequenztechnik
Gustav-Kirchhoff-Str. 4, Berlin 12489, Germany
E-mail: anna.mogilatenko@fbh-berlin.de

Dr. A. Mogilatenko, J. Weinrich
Institute of Physics
Humboldt-University of Berlin
Newtonstr. 15, Berlin 12489, Germany

L. Cancellara
Leibniz-Institut fuer Kristallzuechtung
Max-Born-Straße 2, Berlin 12489, Germany

The ORCID identification number(s) for the author(s) of this article can be found under https://doi.org/10.1002/crat.201900215

DOI: 10.1002/crat.201900215

In this study we will discuss the influence of AlN templates on the relaxation mechanisms during nonpseudomorphic growth of $Al_{0.5}Ga_{0.5}N$ layers for UVB LEDs. Basing on the recent approaches for improvement of structural quality of AlGaN-based LEDs[6,11,12] and the observation of typical, different growth behavior depending on the used AlN/sapphire template, three templates were chosen: AlN/sapphire templates grown on sapphire with an offcut of 0.2° and 0.5° to the sapphire m-plane and an HTA-treated AlN/sapphire template. Our analysis suggests that for decreasing Al content in AlGaN even small differences in TDDs as well as the strain state of the underlying AlN templates can have a strong influence on the relaxation mechanisms of the AlGaN layers.

In situ reflectometry at 280 nm and curvature measurements will be shown to identify the different phases of strain relaxation and the related surface roughening during $Al_{0.5}Ga_{0.5}N$ growth. The different curvature as well as the reflectivity behavior during the growth of an UVB-LED structure on different types of AlN templates will be correlated to the different structural properties of the templates investigated by atomic force microscopy (AFM) and transmission electron microscopy (TEM) as well as by X-ray diffraction (XRD).

2. Experimental Section

The LED heterostructures were grown by metalorganic vapor phase epitaxy (MOVPE) using standard precursors simultaneously on three different two inch (0001) oriented AlN/sapphire templates in a Close Coupled Showerhead reactor. The LED structures consist of 125 nm homoepitaxial AlN, a 200 nm thick AlN/GaN short-period superlattice (SL) resulting in average in $Al_{0.95}Ga_{0.05}N$ followed by 600 nm undoped $Al_{0.75}Ga_{0.25}N$, 1600 nm $Al_xGa_{1-x}N$ graded from $x = 0.75$ to $x = 0.5$, a thick 750 nm n^--$Al_{0.5}Ga_{0.5}N$:Si buffer, and 1150 nm n-$Al_{0.5}Ga_{0.5}N$:Si contact layer. On this n-side the active region consisting of three InAlGaN/InAlGaN multiquantum wells (MQWs) for 310 nm emission is grown followed by a 16 nm thick Mg-doped AlGaN electron blocking layer,[13] 100 nm thick p-$Al_{0.4}Ga_{0.6}N$:Mg, and a 30 nm thick p^+-GaN:Mg contact layer. For p-type activation the samples were annealed in situ at 890 °C for 15 min in nitrogen ambient. The MOVPE growth was monitored by a LayTec EpiCurveTT in situ metrology system measuring 405 nm reflectance and curvature of the wafers. Additionally, a 280 nm reflectance system was installed, since the in situ reflectometry sensors working in the blue-violet wavelength region reach their limits for the InAlGaN system concerning their sensitivity to surface roughening. The layer thicknesses were determined by Fabry–Perot oscillations of the in situ reflectivity data at 405 nm and additionally assessed ex situ by scanning electron microscopy (SEM) of sample cross-sections using backscattered electron imaging.

Strain, degree of relaxation and layer compositions were determined by high-resolution XRD (HRXRD) using ω–$\omega/2\theta$ reciprocal space maps (RSM) of the (00.4) and (11.4) reflections as well as X-ray diffraction omega rocking curves in (00.2) and (10.2) reflection in a PANanalytical X'Pert^3 system including a fourfold 220 Ge monochromator. For rocking curve measurements, the aperture on the source side was 0.5 mm × 5 mm and the acceptance angle in front of the detector was 1°. For RSM measurements an array detector was used.

The surface morphology of the AlN templates was investigated by AFM in contact mode. Structural sample characterization was carried out by SEM and TEM including diffraction contrast analysis and scanning transmission electron microscopy (STEM). For analysis of spatial dislocation distribution STEM was used in strain sensitive annular dark-field (ADF) mode with small acceptance angle. Z-contrast images were acquired by high angle annular dark-field (HAADF) STEM.

Nominally identical UVB-LED heterostructures were grown simultaneously on three AlN/sapphire template layers with different TDD and different surface roughness. In situ reflectance and curvature traces as well as structural properties of the samples were compared to understand relaxation mechanisms and their dependence on the properties of the template layers.

Templates with 1500 nm thick AlN were grown at elevated temperature[14,15] in a multiwafer reactor on a 430 µm thick sapphire substrate off-oriented by 0.2° and a 0.5° to sapphire m-plane.[16] These AlN base layers show typical full width at half maximum of X-ray rocking curves (XRC-FWHM) of ≈ (60 ± 5) arcsec for the (00.2) reflection for both off-cut angles. The FWHM of the (10.2) reflection is (600 ± 15) arcsec for the 0.2° off-cut and (550 ± 15) arcsec for the 0.5° off-cut sample. The estimated total TDD[17–19] is $(4 \pm 0.2) \times 10^9$ cm^{-2} and $(3 \pm 0.2) \times 10^9$ cm^{-2}, respectively. The applied TDD calculation procedure provides reliable results, since the estimated TDDs correlate well with TDDs determined by defect etching with a KOH solution (analyzed area of 10 µm x 10 µm) and dark spot densities determined by cathodoluminescence (CL) spectroscopy.[20,21]

Additionally, a 400 nm thick AlN grown by MOVPE on sapphire with an off-cut of 0.1° to m-plane was treated by HTA and subsequently overgrown with a 450 nm thick MOVPE AlN layer,[20] called as HTA-AlN template. For HTA the temperature was kept at 1710 °C for 3 h to obtain a TDD of $(1 \pm 0.2) \times 10^9$ cm^{-2} (XRC-FWHM < (50 ± 5) arcsec for the (00.2) reflection and (390 ± 15) arcsec for the (10.2) reflection). These FWHM values as well as diffraction contrast analysis in TEM (not shown here) proved that in all AlN templates the majority of threading dislocations (TDs) corresponds to the edge-type, whereas the density of screw- and mixed-type TDs is at least one order of magnitude lower.

The surface morphology of the different AlN/sapphire templates is shown in **Figure 1**a–c. The templates with a TDD of $(4 \pm 0.2) \times 10^9$ (Figure 1a) and $(1 \pm 0.2) \times 10^9$ cm^{-2} (Figure 1c) show bilayer steps, while the 0.5° off-oriented template (Figure 1b) with a TDD of $(3 \pm 0.2) \times 10^9$ cm^{-2} has a step-bunched surface with about 6 nm high steps.[16]

The initial strain in the basal plane of the AlN templates was estimated by HRXRD at room temperature (RT). It corresponds to −0.19% for both nonannealed templates shown in Figure 1a,b (i.e., the lattice constant a of the AlN template is 0.3105 nm compared to the bulk value of 0.3111 nm[22]) and to −0.34% for the HTA AlN template (the lattice constant $a = 0.3100$ nm). The decrease in in-plane lattice constant of HTA AlN has been reported and is mainly defined by the heating temperature and duration.[6]

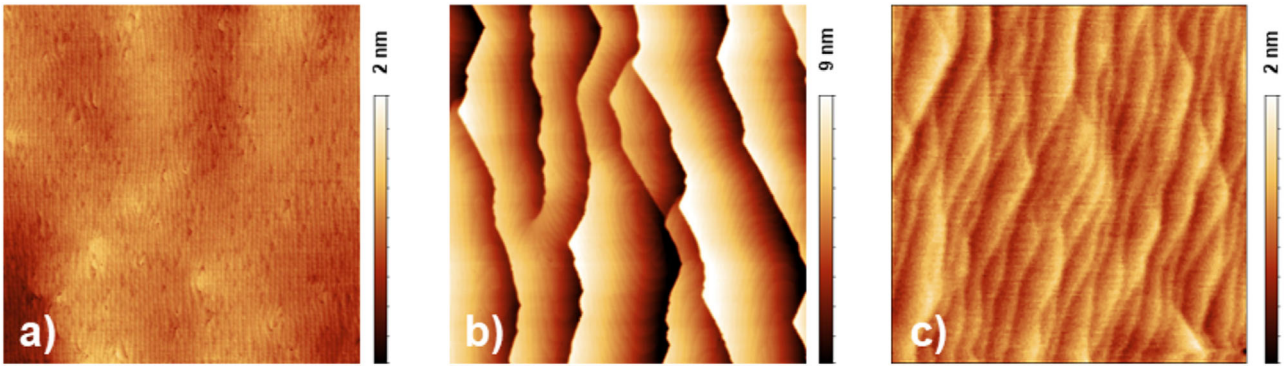

Figure 1. AFM images (5 μm × 5 μm) of c-plane oriented AlN/sapphire templates with TDD of: a) $(4 \pm 0.2) \times 10^9$ cm^{-2} on sapphire with 0.2° off-cut to m-plane, b) $(3 \pm 0.2) \times 10^9$ cm^{-2} on sapphire with 0.5° off to m, and c) $(1 \pm 0.2) \times 10^9$ cm^{-2} on sapphire 0.1° off to m (400 nm AlN annealed for 3 h in N_2 at 1710 °C and overgrown by further 450 nm AlN).

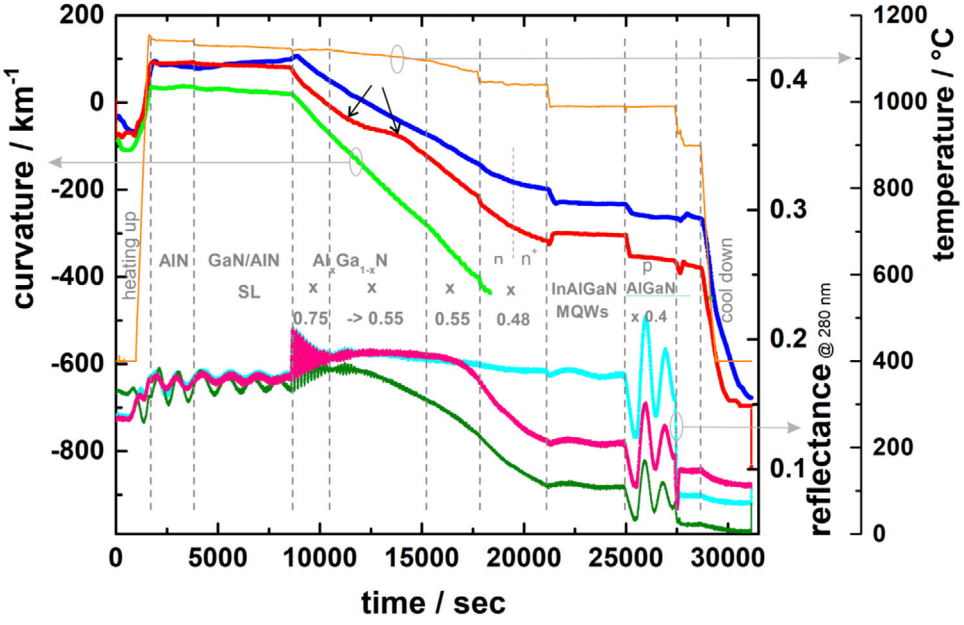

Figure 2. In situ data of MOVPE growth of UVB-LED structure on AlN template with: a) TDD ≈ $(4 \pm 0.2) \times 10^9$ cm^{-2}, blue/cyan data points; b) TDD ≈ $(3 \pm 0.2) \times 10^9$ cm^{-2}, red/pink data; and c) TDD ≈ $(1 \pm 0.2) \times 10^9$ cm^{-2} (HTA-AlN template), green data. Left side: curvature and right side: reflectance at 280 nm (R_{280}) and growth temperature (orange).

3. Results and Discussion

The in situ data (growth temperature, 280 nm reflectance (R_{280}) as well as the curvature (K)) during the MOVPE growth of the UVB-LED structure on the three different AlN templates are shown in **Figure 2**. For a constant Al mole fraction of the growing AlGaN layer the slope of the curvature should be constant and is determined by the Al-content of the layer as long as it grows pseudomorphically. For decreasing Al mole fractions the lattice mismatch of the AlGaN layer to the AlN template and so the compressive strain increase, and the negative slope of curvature should increase.

The cyan/blue graphs in Figure 2 illustrate the in situ data of the growth on the template with the highest dislocation density and a smooth surface (Figure 1a). Rather untypically, during growth of the AlN/GaN superlattice the curvature (blue graph, upper part of Figure 2) increases, i.e., tensile stress is induced during the growth of this layer, although the addition of GaN is generally expected to introduce compressive strain in the structure. According to XRD measurements at RT the AlN template is slightly compressively strained with the in-plane strain ε_a of about only 0.19%. Due to thermal expansion this strain value is compensated at the growth temperature and the AlN/GaN SL with the average $Al_{0.95}Ga_{0.05}N$ concentration should grow nearly unstrained (see red and green curvature curves of other samples in the region of AlN/GaN SL). In contrast, a fit of the curvature slope by Stoney's equation delivered a tensile strain of 0.4%, which is much higher as expected. Thus thermal

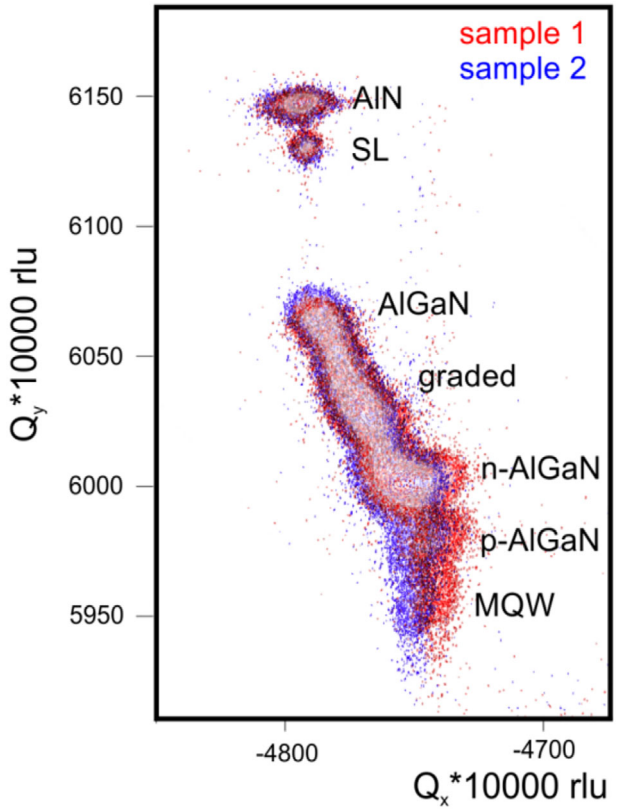

Figure 3. RSM in (11.4) reflection of LED structures on AlN template with TDD of $(4 \pm 0.2) \times 10^9$ cm^{-2} (sample 1) and $(3 \pm 0.2) \times 10^9$ cm^{-2} (sample 2).

expansion cannot explain the observed increase in curvature. This unusual observation suggests that effective lattice constant of the AlN/sapphire pseudosubstrates (see ref. [20]) might be larger than the lattice constant of the SL with an average Al-content x of 0.95. But the reason for this remains unclear. The relaxation degree of the SL determined ex situ from RSM was (18 ± 3)% (**Figure 3**). As this means a relaxation of compressive strain the authors assume this strain to be released at a later moment of growth, when compressive strain of the upper layers is released for example by dislocation motion.

The AlN/GaN SL is followed by an $Al_{0.75}Ga_{0.25}N$ layer, where the curvature decreases linearly as expected for the compressive growth of AlGaN with a constant Al mole fraction. In the following $Al_xGa_{1-x}N$ layer the Al-content is linearly graded from $x = 0.75$ to $x = 0.5$ by reducing the growth temperature (see orange curve). This reduces the loss of Ga due to desorption and thus the Al mole fraction. The curvature decreases further nearly linearly, i.e., the slope stays nearly constant. However, the compositional grading of the Al-content in the AlGaN layer should lead to a constant negative *increase* of the slope and also the lowering of the growth temperature should act in the same direction. Thus, the observed constant slope shows that strain relaxation takes place during the growth of the graded AlGaN. The relaxation degree of the graded layer increases from 18% to 53% as determined from RSM (Figure 3).

During the subsequent growth of the n^+-AlGaN:Si contact layer with a constant composition the curvature slope decreases. Such behavior is known for interaction of Si with dislocations.[23–25] The ex situ determined relaxation degree of the layer increased up to a value of 78%. During the growth of the active region and the p-side the curvature decreases further with a small negative slope because of the slow growth rates and the lower Al mole fractions in comparison to the (partially) relaxed $Al_{0.5}Ga_{0.5}N$ underlayer. The reflectance (cyan data points, lower part of Figure 2) does not show any significant roughening during the growth of the AlGaN buffer or of the nonpseudomorphically grown *n*-contact layer and the p-side. At the end of the growth process during the cooling down the curvature decreases drastically because of the larger thermal expansion coefficient of the sapphire in comparison to that of the AlGaN layers, i.e., the wafer becomes strongly convexly bowed and the whole structure is compressively strained.

Figure 4 shows the cross-sectional ADF STEM images of the first layers of the UVB-LED structure grown on the AlN template with the highest TDD of $(4 \pm 0.2) \times 10^9$ cm^{-2}. The near-surface region of the AlN template, the homoepitaxial AlN, the AlN/GaN SL, and the bottom of the $Al_{0.75}Ga_{0.25}N$ buffer layer are visible. This ADF STEM image was obtained in the [11–20] AlN viewing direction and shows all dislocation types formed in the sample.

In the pseudomorphically grown AlN/GaN SL the vertical dislocation lines are slightly inclined to relax the strain of the SL with an average Al-concentration of $x = 0.95$ (Figure 4a). The inclination angle increases further when the Al content decreases, i.e., at the interface between the AlN/GaN superlattice and the subsequent $Al_{0.75}Ga_{0.25}N$ buffer layer. As shown by Follstaedt et al.[26] such dislocation line inclination provides relaxation of compressive strain in AlGaN layers on AlN, since the projected length of an inclined dislocation onto the interfacial c-plane acts as a misfit dislocation segment. A summary of the observed inclination angles as well as their contribution to the strain relaxation is given in **Table 1**.

Nevertheless, we observe one distinct difference compared to "bulk" AlGaN growth on AlN. There is a formation of horizontal dislocation lines within the AlN/GaN superlattice (Figure 4a,c). It is expected that at least some of them are formed after the SL growth during the growth of the more compressively strained $Al_{0.75}Ga_{0.25}N$ or the graded AlGaN layer. Note that there is a number of the horizontal dislocations appearing at different thickness in the AlN/GaN SL and even in the AlN underneath (Figure 4a). Furthermore, the dislocation lines are not straight but contain a number of pinned positions formed due to intersections with vertical TD lines (see the dashed arrows in Figure 4a). Analyzing the shape of the dislocation lines, we conclude that movement of the horizontal dislocations takes place toward the AlN template during the growth to release the increasing compressive strain. Diffraction contrast images in Figure 4b,c show one and the same specimen area imaged using two-beam conditions and visualizing TDs with a screw (Figure 4b) and an edge component (Figure 4c) of the Burgers vector. These images suggest that the Burgers vector of the horizontal dislocations lies in the c-plane, which confirms their ability for strain accommodation.

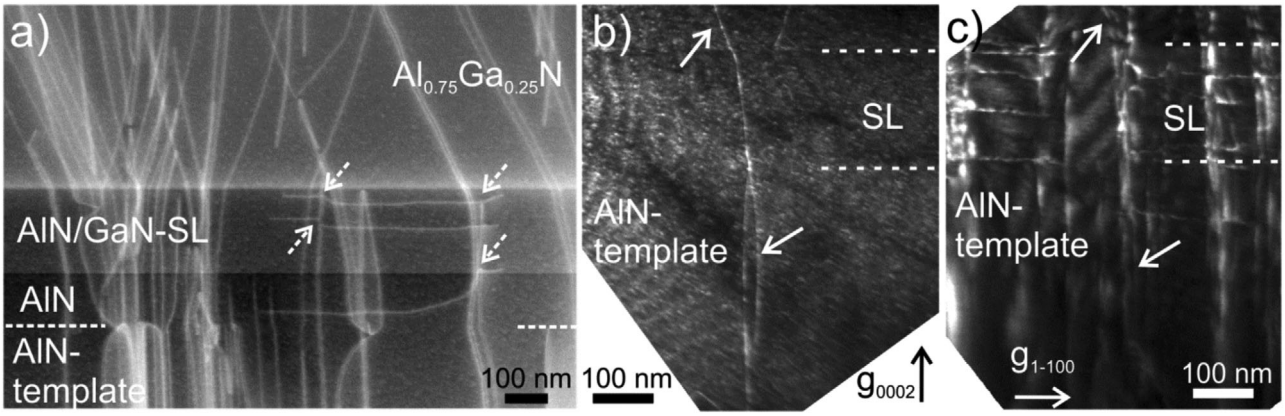

Figure 4. Exemplary cross-sectional images of lower part of UVB-LED structure on AlN template with TDD of $(4 \pm 0.2) \times 10^9$ cm^{-2}: a) ADF STEM showing formation of horizontal dislocation lines in AlN/GaN superlattice and strong TD inclination in subsequently grown AlGaN (viewed in [11-20]AlN projection). b,c) Dark-field diffraction contrast images of the same specimen area visualizing different types of defects (white arrows indicate the same specimen positions).

Table 1. Calculation of relative relaxation in the superlattice and the following AlGaN layers. The calculation of the relaxation by TD inclination is based on ref. [36].

Template	Layer composition x (± 0.02)	Inclination angle [°] (± 3°)	Relaxation [%]	
			By TD inclination	Based on XRD (± 3%)
0.2° offcut	0.95	10	9 ± 3	18
	0.58	16	52 ± 9	53
0.5° offcut	0.94	8	5 ± 2	26
	0.60	23	55 ± 9	49
HTA-AlN	0.95 ± 0.03	19	1.1 ± 0.3	–
	0.65 ± 0.07	30	25 ± 6	–

During the further AlGaN growth, at the interface between the SL and the $Al_{0.75}Ga_{0.25}N$ layer the inclination of the dislocations is increased because of the increased compressive strain (Figure 4a). The degree of relaxation (RSM) increases to (53 ± 3)% during the grading of the Al-content and further to (78 ± 3)% in the *n*-$Al_{0.5}Ga_{0.5}N$ layer. Both, the observed TD line inclination, the formation of horizontal dislocation lines and their movement into the substrate should effectively reduce the strain in the system, which results in the constant curvature slope observed for graded AlGaN layer, where the increasing Ga content should generally lead to the slope changes, as discussed above.

The following layers grew pseudomorphically on the *n*-$Al_{0.5}Ga_{0.5}N$ layer as confirmed by RSM measurement (Figure 3). No generation of new dislocations was observed. Spatially resolved cathodoluminescence investigation of the MQW-region in top view[16] showed a TDD reduced down to about (1–2) × 10^9 cm^{-2}, which is achieved by mutual annihilation and must be supported by the strong line inclination in the 4.5 µm thick AlGaN layer below the MQWs.

Summarizing the observed results, the growth of UVB LED structure on AlN/sapphire template with a smooth surface and a TDD of $(4 \pm 0.2) \times 10^9$ cm^{-2} leads to such classical relaxation mechanisms as TD inclination as well as formation and climb of horizontal dislocations.

In contrast to the previous sample, the growth on the AlN template with a TDD of $(3 \pm 0.2) \times 10^9$ cm^{-2} and a stepped surface morphology (Figure 1b) leads to a different relaxation behavior (Figure 2).

The red graphs in Figure 2 show the in situ data of this sample. In this case the SL grows compressively strained as expected (negative slope of curvature, red line). The most prominent difference between the two templates is their different surface morphology and connected with that a slightly reduced TDD. ADF STEM analysis (**Figure 5**a) shows the same relaxation effects (i.e., TD inclination and formation of horizontal dislocation lines) in the AlN/GaN SL as in the previous sample grown on the template with a smaller offcut. In contrast, strain relaxation reaches a value of (26 ± 3)% in the SL as determined by RSM (Figure 3). The higher relaxation can be generally achieved by a stronger inclination angle of TD lines. However, our analysis of inclination angles does not show any strong difference compared to the previous sample (Table 1). This suggests that the formation of horizontal dislocation segments in the SL can be more enhanced in this sample.

In the in situ curvature measurements the main differences appear right after the beginning of the growth of the graded AlGaN layer: the curvature slope decreases till the middle of the layer (see the small plateau marked by arrows in the red curve) indicating that further relaxation processes are taking place. In the second half of the growth of this layer the negative slope increases again. The relaxation seems to decay and the decreasing Al mole fraction induces increasing compressive strain again. After 2/3 of the layer thickness the curvature slope becomes again constant with a similar slope value as in the beginning of the growth. R_{280} stays constant, indicating that the observed decrease in compressive strain during the growth of the graded layer is not correlated with a significantly increased surface area by a change to a 3D columnar growth mode. Thus, the observed relaxation must be induced by a different relaxation mechanism than 3D growth, e.g., by formation of new crystal defects.

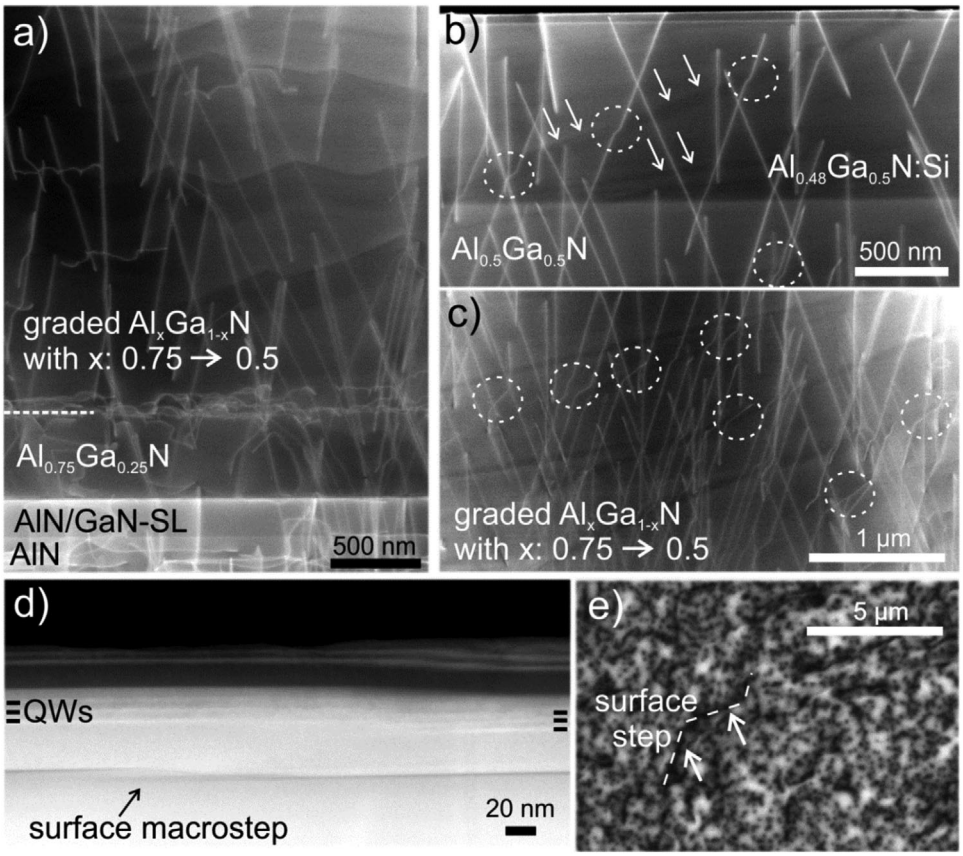

Figure 5. Results of structural analysis of UVB-LED structure on AlN template with TDD of $(3 \pm 0.2) \times 10^9$ cm^{-2} and off-cut of 0.5° to m: a) ADF STEM image in [1-120]AlN zone axis showing formation of horizontal defect band in graded AlGaN layer. b) ADF STEM image in [1-100]AlN zone axis showing inclined TDs in the upper part of the LED and c) in the lower part of graded AlGaN (white arrows show dark inclined specimen regions due to Ga enrichment on macrostep sidewalls; dashed circles show the positions where TDs interact with macrosteps). d) HAADF STEM image in [1-100]AlN zone axis showing macrostep in active region of the LED. e) Monochromatic CL image obtained at 308 nm from the surface of active region (white arrows show surface macrosteps appearing dark due to Ga enrichment).

Indeed, ADF STEM analysis (Figure 5a) shows that a bunch of horizontal dislocations is formed at the interface to the graded AlGaN layer. Diffraction contrast experiments showed that these dislocations exhibit an *a*-component of the Burgers vector. Thus, they will contribute to strain relaxation. Similarly to the previous sample, we suggest that these dislocations are not initially formed at this interface but are produced during the increasing thickness of the graded AlGaN layer and climb down to this interface. We conclude that, when the TDD is slightly lower, the strain relaxation mechanisms present in the previous sample are not sufficient to relax the compressive strain of the graded AlGaN layer. During the AlGaN growth on AlN with a reduced TDD the same amount of compressive strain relaxation would require higher TD line inclination angles and thus longer dislocation line lengths projected onto the interfacial plane, which is not the case (Table 1). This can be the reason for the start of the formation of the horizontal dislocation bunches.

This relaxation process is most probably supported by TD interaction with the sidewalls of macrosteps which move across the sample surface as the growth proceeds (Figure 5b,c). As the macrosteps provide a free sidewall, the TDs appearing close to them are attracted by the image force. Those TDs then follow the macrostep during the growth for some distance (see the strongly inclined segments of TD lines marked by dashed circles in Figure 5b,c). This strong local inclination provides a larger dislocation projection length on the growth plane and thus can locally contribute to the strain relaxation.

Furthermore, the presence of surface macrosteps, stemming already from the AlN template, can lead to an enhanced Ga incorporation on the macrostep edges. The more mobile Ga adatoms will be preferentially incorporated at the step sidewalls leading to composition inhomogeneities (visible as dark inclined regions in ADF STEM images in Figure 5b,c) and a higher growth rate as it was shown in earlier works.[16,11,27] These Ga rich regions can act as localized roughening sites providing a larger surface. Nevertheless, in this sample the total macrostep contribution to the strain relaxation should not be strong, since the total inclination angle of the TDs after the interaction with macrosteps is similar to that of TDs which did not undergo any interaction. Furthermore, at the beginning of the AlGaN growth the macrosteps are higher, the Ga-rich regions are more extended, and the strongly inclined TD segments are longer (Figure 5b,c).

Both, the macrosteps and the Ga-rich regions on them fade away as the growth proceeds and their contribution to the relaxation process should decrease.

During the growth of the nonpseudomorphic $Al_{0.5}Ga_{0.5}N$ n-contact layer R_{280} (red lines, lower part of Figure 2) starts to decrease significantly. Nevertheless, the curvature decreases further nearly linearly showing that the strain is not mainly released by increase of the surface area via 3D growth. Instead, the initially 6 nm high surface steps (Figure 1b) develop into terraces with expanded inclined sidewalls as known for templates with off-cut angles from c-plane larger than 0.25°.[16,11] The curvature during the AlGaN growth decreases with a higher slope (more compressive strain) in comparison to the growth on the template with the higher TDD and smoother surface, which leads to a stronger convex bow during the growth of the MQWs ($-330\ km^{-1}$ vs $-200\ km^{-1}$).

In the HAADF STEM image of Figure 5d an extended inclined macrostep can be seen below the MQWs. The presence of the macrosteps leads to disturbed MQW regions. The number of vertically directed threading dislocations is not dramatically decreased and the TDD in the MQWs reaches about $(1 \pm 0.2) \times 10^9\ cm^{-2}$ as was confirmed by CL measurements. The monochromatic CL map (Figure 5e) was acquired at a wavelength of 308 nm, thus the macrostep edge with a Ga-enrichment at the step edge appears as a dark line in this CL image. The Ga enrichment leads to a longer emission wavelength and so to an increased full width at the half maximum of the quantum well (QW) emission peak from 9 nm for the sample with a 0.2° off-cut to about 12–16 nm for the sample on template with a 0.5° off-cut.

Summarizing these results, the growth of UVB LED structure on AlN/sapphire template with a TDD of $(3 \pm 0.2) \times 10^9\ cm^{-2}$ and a stepped surface morphology with the step height of about 6 nm also leads to similar relaxation mechanisms as TD inclination and formation and climb of horizontal dislocations. The macrosteps increase the free layer surface and interact with TDs locally increasing their inclination. Both these processes should support strain relaxation in these layers. Nevertheless, compared to the previous sample, the formation of an additional extended horizontal dislocation bunch takes place at the interface to the graded AlGaN layer. We suggest that the reason for the different relaxation scenario is the slight TDD reduction.

For the growth of the UVB-LED structure on the HTA-AlN template with the lowest TDD of $(1 \pm 0.2) \times 10^9\ cm^{-2}$ the in situ data are shown as green data points in Figure 2. Besides the lower TDD, one of the main differences of this AlN template layer is its smaller lattice constant compared to the previous two template layers (i.e., 0.3100 nm for HTA-AlN versus 0.3105 nm for nonannealed AlN). The smaller lattice constant leads to a larger lattice mismatch to $Al_xGa_{1-x}N$ with the same Al content in comparison to nonannealed AlN templates. As result, the x-value for pseudomorphic growth should shift to higher Al contents and the strain relaxation should take place at lower layer thicknesses compared to the growth on nonannealed AlN templates.

Unlike in the previously described samples, in situ curvature measurements show that the curvature decreases with a higher constant negative slope right from the start of the $Al_{0.75}Ga_{0.25}N$ growth. Furthermore, the curvature decrease is observed during the whole graded AlGaN growth despite the changing composition (upper part of Figure 2). R_{280} (green line, lower part in Figure 2) starts to decrease shortly after the start of the graded AlGaN layer. Obviously, during the growth of graded AlGaN the increasing surface roughening, indicated by R_{280}, does not have any impact on the evolution of the wafer curvature and does not provide any significant relaxation. In the further growth the surface roughening becomes so pronounced that reflectance values decrease down to a level, were the reflected spots for the curvature measurement cannot be detected anymore (see green line in upper part of Figure 2).

TEM analysis was applied to identify the processes taking place in the defect structure of this sample (**Figure 6**). An exemplary cross-sectional ADF-STEM image in Figure 6a shows a lower part of this LED sample. As visible, TD lines in the HTA-AlN template are rather curved in comparison to nonannealed AlN templates (e.g., Figure 4), where the TD lines are vertical or slightly inclined, but mostly rather straight. This curved shape of the TD lines indicates the climbing processes, which took place at high HTA temperatures (1710 °C) and resulted in an enhanced TD annihilation and TDD reduction down to $1 \times 10^9\ cm^{-2}$. Overgrowth by AlN using MOVPE shows the formation of misfit dislocations and irregular dislocation lines which appear at the homoepitaxial interface. Additionally, the TDs of the initial template are inclined at the homoepitaxial interface (see black arrows in Figure 6a). These both findings indicate the presence of a stress component, which can arise when the a-lattice constant of the HTA-AlN is smaller than that of the MOVPE-grown AlN buffer layer of the LED structure. Additionally, the reduced TDD minimizes the possibility to relax the compressive strain only by dislocation line inclination.

According to the curvature measurements the subsequently grown SL with an average Al-content of 95% is slightly compressively strained (Figure 2). The increasing inclination of the TD lines with increasing Al-content (Table 1) as well as the formation of individual nearly horizontally arranged dislocation lines with an irregular shape indicate similar relaxation processes as for the previous samples. In contrast, despite the higher inclination angles of TDs (Table 1), the following $Al_{0.75}Ga_{0.25}N$ layer shows an enhanced defect formation. In particular, bunches of helical dislocations (i.e., dislocation lines in form of a spiral) appear in this layer (see white arrows in Figure 6a). The formation of helical dislocations was rarely reported in group-III nitrides, mostly either during coalescence of laterally overgrown GaN layers[28] or in ammonothermal GaN.[29] It was shown that in GaN with low TDDs TDs with initially vertical dislocation lines and a screw component of the Burgers vector can be transformed into helical dislocations at elevated temperatures.[29] Diffraction contrast analysis proved that in our sample the helical dislocations have both c- and a-component of the Burgers vector. Vacancy absorption by straight dislocation lines was proposed to be the mechanism responsible for this transformation. Interestingly, this transformation seems to take place only when the number of TDs is low.[28,29] We suggest that in our samples this process appears in the already grown AlGaN layer with initially straight TD lines. A simultaneous action of a number of parameters must be responsible for this process: high growth temperatures, the presence of high compressive stress due to the overgrowth with AlGaN with a lower Al-content, the presence of a relatively low TDD, which could accommodate this strain, and an excess of point defects, which are necessary for this climb process and transformation

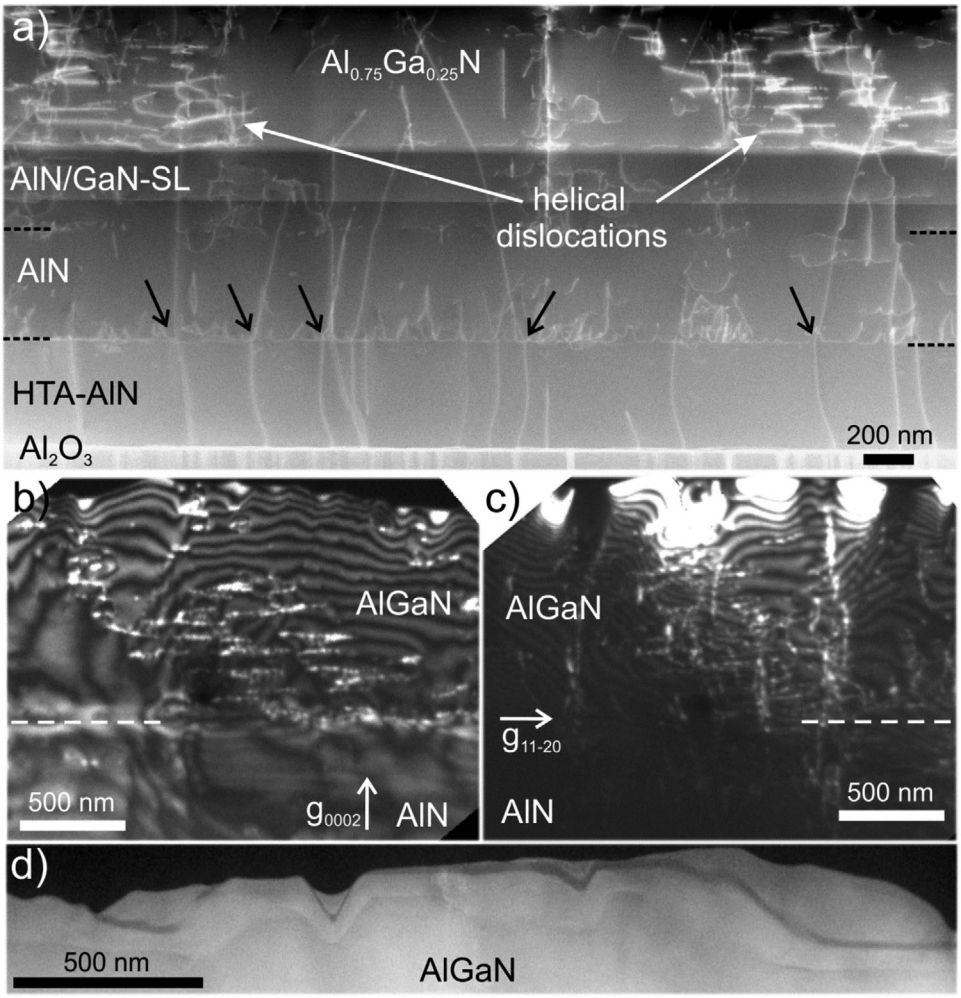

Figure 6. a) ADF STEM cross-sectional image showing defect behavior in the first layers of a UVB-LED structure grown on HTA-AlN template with TDD $\approx 1 \times 10^9$ cm^{-2}. b,c) Diffraction contrast images proving the presence of both *c*- and *a*-component of the Burgers vector of helical dislocations in AlGaN. d) HAADF STEM image of sample surface proving the strain relaxation by surface enlargement.

to the helical shape. HTA-annealed AlN can be a source of such point defects.[30] Generally, the formation of helical dislocations is not necessarily a strain induced process, but can occur at high temperatures at the simultaneous point defect oversaturation. However, in this sample the main axis of the helices is strongly inclined with respect to the *c*-axis, which suggests that they can have a certain contribution to the strain relaxation.

Nevertheless, this transformation and its possible contribution to the strain relaxation is not enough to release the large and even further increasing lattice mismatch during the following Al-grading. This leads to the strain relaxation by a surface enlargement by formation of individual macrofacets and causes a destruction of the MQWs. Obviously, the growth conditions optimized for the growth on AlN templates with TDD of mid 10^9 cm^{-2} are not suitable for the successful growth of UVB-LED structures on low TDD HTA-AlN templates. Here one has to take into account the lower lattice constants and the lower TDD of the HTA-AlN (in comparison to MOVPE-grown AlN). A possible way to reduce the strong compressive strain in the nonpseudomorphic AlGaN would be the change of the growth mode to a 3D mode as it was shown for the development of low TDD AlN templates with increased AlN layer thickness[20,31–34] and for UVB-LED structures[10,35] as well as recently for the deposition of $Al_{0.55}Ga_{0.45}N$ layers for UVB laser structures.[9] However, here the surface needs to be smoothened before the MQW is grown, which again is a challenge.

Summarizing the observed results, since HTA-AlN templates show a decreased TDD of $(1 \pm 0.2) \times 10^9$ cm^{-2} and a decreased lattice constant, relaxation scenario of the AlGaN-based UVB LED layers becomes different. Similarly to the previous samples, there is a relaxation by TD line inclination with increased inclination angles due to the reduced TDD (see Table 1). However, the enhanced inclination is not enough to achieve any significant strain relaxation, which leads to alternative processes such as formation of helical dislocations with inclined bands and enhanced surface enlargement by formation of macrofacets.

Our phenomenological study suggests that even small differences in TDDs as well as the lattice constant of the AlN/sapphire templates have a strong impact on the relaxation processes in the UVB LEDs, whereas the different surface morphology

(i.e., an initial presence of 6 nm high surface steps) plays a secondary role. Table 1 summarizes the results of strain relaxation calculation based on analysis of TD line inclination by[36] as well as the relaxation data obtained from RSM analysis. The TD inclination angles were measured in cross-section on a rather small specimen area of about 4 µm in length. Unfortunately, for the HTA sample it was not possible to perform HRXRD measurements due to the high surface roughness of the sample. Therefore, the Ga content in these layers is a rough estimation based on experience.

Nevertheless, for the samples grown on AlN templates with different offcut angles to the sapphire m-plane the comparison of the RSM data (Figure 3) and the modeled strain release enables a more quantitative understanding of the relaxation process. Apparently, the inclination of TDs in the AlN/GaN SL (corresponding to the $Al_{0.95}Ga_{0.05}N$ composition) cannot provide the relaxation degree estimated from the RSM data. This is a reasonable result since this layer grows nearly unstrained. As the TD inclination is a stress-driven process realized by surface mediated climb, one would not expect this to be strong for such layer compositions on AlN. The higher relaxation found ex situ by XRD can be explained by the role of horizontal dislocations stemming from AlGaN layers with a lower Al content, moving downward and penetrating the SL and the AlN template at a later point of growth due to a higher compressive strain in the subsequently grown AlGaN layers.

In contrast, in the $Al_xGa_{1-x}N$ layer grown after the compositional grading up to about $x = 0.55$ the plastic relaxation predicted by the TD inclination model fits quite well the RSM-based relaxation values. According to this calculation, for the decreased Al content the TD inclination seems to be the main relaxation process. This finding contradicts the results obtained by in situ curvature measurements, which clearly show a different relaxation behavior in both samples. The TD inclination should reflect the in situ changes taking place in the samples at growth temperatures. Thus, its good coincidence with the ex situ measured RSM-based relaxation values is surprising. It should be kept in mind that the TEM-based analysis provides rather poor statistics. For example, strong fluctuations of TD inclination angles were observed due to the presence of TD clusters and in the vicinity of surface steps. Furthermore, the inclination angles tend to vary with increasing layer thickness for a constant Al content and can depend on the offcut direction. Also the additional formation of the horizontally arranged defects and defect bands is a clear evidence for the fact that the TD inclination alone is not enough for the strain relaxation.

As expected, a decrease in TDD down to $(1 \pm 0.2) \times 10^9$ cm^{-2} by using an HTA-AlN template results in larger inclination angles compared to the higher TDDs. Even though this increased TD inclination leads to a much lower relaxation as the total TDD is too low. As result, at a certain point the total strain energy exceeds a critical value and strain relaxation by roughing of the sample surface takes place.

4. Summary

It has been shown that even small changes in the dislocation density and lattice constant of AlN/sapphire templates can lead to very different behavior during the deposition of (Al,Ga)N layer structures required for UVB-LEDs. When the dislocation density in the AlN template is reduced to the low 10^9 cm^{-2} range or even below, the usual relaxation mechanisms such as the formation of misfit dislocations as well as the inclination of vertically directed threading dislocations reach their limits. For decreased TDDs in HTA-AlN/sapphire templates more harmful mechanisms such as dislocation transformation into helical ones accompanied by drastically increased surface roughening takes place. This transformation is the result of the lower TDD, smaller lattice constant of the AlN template as well as an initially higher point defect concentration in HTA-AlN.

The given examples of in situ data and TEM investigations show that for the growth of strongly compressively strained AlGaN layers for UVB-LEDs on AlN templates the relaxation mechanism is strongly influenced by the absolute values of TDD as well as the lattice constants of the AlN/sapphire pseudo-substrates and is less influenced by their surface morphology (at least for roughness values ≤ 6 nm). Obviously, the growth conditions optimized for conventional nonannealed AlN templates with TDD of mid 10^9 cm^{-2} must be further optimized for the successful growth of UVB-LED on HTA-AlN templates with reduced TDDs.

Acknowledgements

The authors would like to thank C. Neumann for technical assistance with the MOVPE machine, H. Lawrenz for the cathodoluminescence, and J. Enslin for the AFM measurements. Furthermore, the authors thank LayTec AG for the support with a 280 nm reflectance system and helpful discussion of in situ data. This study was partially supported by German Federal Ministry of Education and Research (BMBF) through the consortia project "Advanced UV for Life" under contracts 03ZZ0130A, 03ZZ0134C, 03ZZ0130B, and 03ZZ0134B and by the Deutsche Forschungsgemeinschaft (DFG) within the Collaborative Research Center "Semiconductor Nanophotonics" (SFB 787).

Conflict of Interest

The authors declare no conflict of interest.

Keywords

dislocations, group-III nitrides, substrate curvature, UV LED

Received: November 20, 2019
Revised: February 7, 2020
Published online: May 27, 2020

[1] K. Davitt, Y. Song, W. R. Patterson, A. Nurmikko, M. Gherasimova, J. Han, Y. Pan, R. K. Chang, *Opt. Express* **2005**, *13*, 9548.
[2] M. Kneissl, J. Rass, *III-Nitride Ultraviolet Emitters*, Springer Series in Materials Science Vol. 227, Springer International Publishing, Basel, Switzerland **2016**.
[3] M. Kneissl, T. Kolbe, C. Chua, V. Kueller, N. Lobo, J. Stellmach, A. Knauer, H. Rodriguez, S. Einfeldt, Z. Yang, N. M. Johnson, M. Weyers, *Semicond. Sci. Technol.* **2011**, *26*, 014036.

[4] K. Ban, J. Yamamoto, K. Takeda, K. Ide, M. Iwaya, T. Takeuchi, S. Kamiyama, I. Akasaki, H. Amano, *Appl. Phys. Express* **2011**, *4*, 052101.
[5] H. Miyake, G. Nishio, S. Suzuki, K. Hiramatsu, H. Fukuyama, J. Kaur, N. Kuwano, *Appl. Phys. Express* **2016**, *9*, 025501.
[6] H. Miyake, C.-H. Lin, K. Tokoro, K. Hiramatsu, *J. Cryst. Growth* **2016**, *456*, 155.
[7] K. Uesugi, Y. Hayashi, K. Shojiki, H. Miyake, *Appl. Phys. Express* **2019**, *12*, 065501.
[8] N. Susilo, S. Hagedorn, D. Jaeger, H. Miyake, U. Zeimer, C. Reich, B. Neuschulz, L. Sulmoni, M. Guttmann, F. Mehnke, C. Kuhn, T. Wernicke, M. Weyers, M. Kneissl, *Appl. Phys. Lett.* **2018**, *112*, 041110.
[9] Y. Kawase, S. Ikeda, Y. Sakuragi, S. Yasue, S. Iwayama, M. Iwaya, T. Takeuchi, S. Kamiyama, I. Akasaki, H. Miyake, *Jpn. J. Appl. Phys.* **2019**, *58*, SC1052.
[10] M. A. Khan, N. Maeda, M. Jo, Y. Akamatsu, R. Tanabe, Y. Yamada, H. Hirayama, *J. Mater. Chem. C* **2019**, *7*, 143.
[11] K. Kojima, Y. Nagasawa, A. Hirano, M. Ippommatsu, Y. Honda, H. Amano, I. Akasaki, S. F. Chichibu, *Appl. Phys. Lett.* **2019**, *114*, 011102.
[12] M. Kaneda, C. Pernot, Y. Nagasawa, A. Hirano, M. Ippommatsu, Y. Honda, H. Amano, I. Akasaki, *Jpn. J. Appl. Phys.* **2017**, *56*, 061002.
[13] T. Kolbe, A. Knauer, J. Rass, H. K. Cho, S. Hagedorn, S. Einfeldt, M. Kneissl, M. Weyers, *Materials* **2017**, *10*, 1396.
[14] O. Reentilä, F. Brunner, A. Knauer, A. Mogilatenko, W. Neumann, H. Protzmann, M. Heuken, M. Kneissl, M. Weyers, G. Tränkle, *J. Cryst. Growth* **2008**, *310*, 4932.
[15] S. Hagedorn, A. Knauer, F. Brunner, A. Mogilatenko, U. Zeimer, M. Weyers, *J. Cryst. Growth* **2017**, *479*, 16.
[16] T. Kolbe, A. Knauer, J. Enslin, S. Hagedorn, A. Mogilatenko, T. Wernicke, M. Kneissl, M. Weyers, *J. Cryst. Growth* **2019**, *526*, 125241.
[17] P. Gay, P. B. Hirsch, A. Kelly, *Acta Metall.* **1953**, *1*, 315.
[18] T. Metzger, R. Höpler, E. Born, O. Ambacher, M. Stutzmann, R. Stömmer, M. Schuster, H. Göbel, S. Christiansen, M. Albrecht, H. P. Strunk, *Philos. Mag. A* **1998**, *77*, 1013.
[19] S. R. Lee, A. M. West, A. A. Allerman, K. E. Waldrip, D. M. Follstaedt, P. P. Provencio, D. D. Koleske, C. R. Abernathy, *Appl. Phys. Lett.* **2005**, *86*, 241904.
[20] S. Walde, S. Hagedorn, M. Weyers, *Jpn. J. Appl. Phys.* **2019**, *58*, SC1002.
[21] S. Hagedorn, S. Walde, N. Susilo, C. Netzel, N. Tillner, R.-S. Unger, P. Manley, E. Ziffer, T. Wernicke, Ch. Becker, H.-J. Lugauer, M. Kneissl, M. Weyers, *Phys. Status Solidi A* **2020**, *2020*, 1900796.
[22] M. Tanaka, S. Nakahata, K. Sogabe, H. Nakata, M. Tobioka, *Jpn. J. Appl. Phys.* **1997**, *36*, L1062.
[23] F. Brunner, A. Mogilatenko, V. Kueller, A. Knauer, M. Weyers, *J. Cryst. Growth* **2013**, *376*, 54.
[24] I. C. Manning, X. Weng, J .D. Acord, M. A. Fanton, D. W. Snyder, J. M. Redwing, *J. Appl. Phys.* **2009**, *106*, 023506.
[25] J. Weinrich, A. Mogilatenko, F. Brunner, Ch. Koch, M. Weyers, *J. Appl. Phys.* **2019**, *126*, 085701.
[26] D. M. Follstaedt, S. R. Lee, A. A. Allerman, J. A. Floro, *J. Appl. Phys.* **2009**, *105*, 083507.
[27] A. Knauer, V. Kueller, U. Zeimer, M. Weyers, C. Reich, M. Kneissl, *Phys. Status Solidi A* **2013**, *210*, 451.
[28] Z. Lilienthal-Weber, M. Benamara, W. Swider, J. Washburn, J. Park, P. A. Grudowski, C. J. Eiting, R. D. Dupius, *MRS Internet J. Nitride Semicond. Res.* **1999**, *4*, 459.
[29] K. Horibuchi, S. Yamaguchi, Y. Kimoto, K. Nishikawa, T. Kachi, *Semicond. Sci. Technol.* **2016**, *31*, 034002.
[30] W. Wei-Ying, J. Peng, L. Gui-Peng, L. Wei, L. Bin, L. Xing-Fang, W. Zhan-Guo, *Chin. Phys. B* **2014**, *23*, 087810.
[31] M. Imura, K. Nakano, N. Fujimoto, N. Okada, K. Balakrishnan, M. Iwaya, S. Kamiyama, H. Amano, I. Akasaki, T. Noro, T. Takagi, A. Bandoh, *Jpn. J. Appl. Phys.* **2006**, *45*, 8639.
[32] N. Okada, N. Kato, S. Sato, T. Sumii, T. Nagai, N. Fujimoto, M. Imura, K. Balakrishnan, M. Iwaya, S. Kamiyama, H. Amano, I. Akasaki, H. Maruyama, T. Takagi, T. Noro, A. Bandoh, *J. Cryst. Growth* **2007**, *298*, 349.
[33] X. Zhang, F. J. Xu, J. M. Wang, C. G. He, L. S. Zhang, J. Huang, J. P. Cheng, Z. X. Qin, X. L. Yang, N. Tang, X. Q. Wangab, B. Shen, *CrystEngComm* **2015**, *17*, 7496.
[34] H. Hirayama, T. Yatabe, N. Noguchi, T. Ohashi, N. Kamata, *Appl. Phys. Lett.* **2007**, *91*, 071901.
[35] J. Enslin, F. Mehnke, A. Mogilatenko, K. Bellmann, M. Guttmann, Ch. Kuhn, J. Rass, N. L. Ploch, T. Wernicke, M. Weyers, M. Kneissl, *J. Cryst. Growth* **2017**, *464*, 185.
[36] A. E. Romanov, J. S. Speck, *Appl. Phys. Lett.* **2003**, *83*, 2569.